

Effective reinforcement in carbon nanotube–polymer composites

BY W. WANG¹, P. CISELLI^{1,2}, E. KUZNETSOV³, T. PEIJS^{1,2}
AND A. H. BARBER^{1,*}

¹*Department of Materials, Queen Mary, University of London,
Mile End Road, London E1 4NS, UK*

²*Eindhoven Polymer Laboratories, Eindhoven University of Technology,
5600 MB Eindhoven, The Netherlands*

³*NT-MDT Co., Zelenograd, Moscow 124460, Russia*

Carbon nanotubes have mechanical properties that are far in excess of conventional fibrous materials used in engineering polymer composites. Effective reinforcement of polymers using carbon nanotubes is difficult due to poor dispersion and alignment of the nanotubes along the same axis as the applied force during composite loading. This paper reviews the mechanical properties of carbon nanotubes and their polymer composites to highlight how many previously prepared composites do not effectively use the excellent mechanical behaviour of the reinforcement. Nanomechanical tests using atomic force microscopy are carried out on simple uniaxially aligned carbon nanotube-reinforced polyvinyl alcohol (PVA) fibres prepared using electrospinning processes. Dispersion of the carbon nanotubes within the polymer is achieved using a surfactant. Young's modulus of these simple composites is shown to approach theoretically predicted values, indicating that the carbon nanotubes are effective reinforcements. However, the use of dispersant is also shown to lower Young's modulus of the electrospun PVA fibres.

Keywords: carbon nanotube; composite; nanomechanics; electrospinning; polymer

1. Introduction

Polymer composites reinforced with strong, high Young's modulus fibres are an important class of lightweight materials often characterized by excellent specific mechanical properties. High aspect ratio fibres added to a polymer matrix increase both Young's modulus and strength of the composite using a stress transfer mechanism from the matrix to the fibre during external loading. The principle of reinforcement in fibre composites uses the assumption that, at a given composite strain, the fibre carries more stress than the matrix since it is stiffer. The use of long fibres in polymer matrices can create composites with a strength and stiffness comparable to metals at a fraction of the weight. However, long fibres are often easily broken up during composite manufacturing. The use

* Author for correspondence (a.h.barber@qmul.ac.uk).

One contribution of 7 to a Theme Issue 'Nanotribology, nanomechanics and applications to nanotechnology II'.

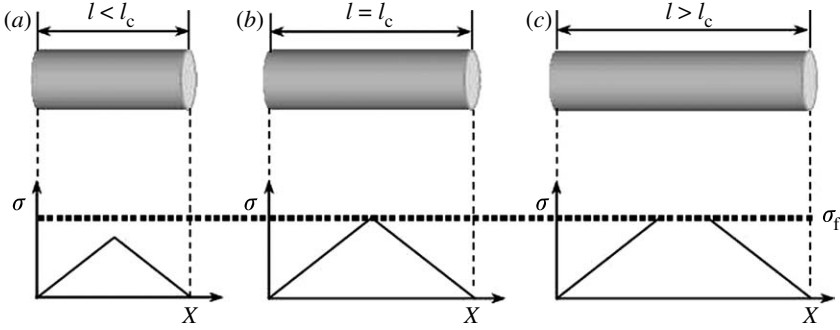


Figure 1. The tensile stress profile in fibres of three different lengths during composite straining. (a) Short fibres have insufficient length to reach the failure stress of the fibre σ_f as indicated by the dotted line, whereas fibres of (b) critical fibre length l_c or (c) greater can fracture.

of short fibres makes the processing of the material easier but makes the reinforcement carry less load. This can be illustrated by considering a single fibre within a polymer matrix under strain. Figure 1 shows the tensile stress transfer profile along the fibre length during composite straining.

The stress builds up along the fibre length, as shown in figure 1, for three different lengths. For the shortest fibre length, the stress builds up until a maximum is reached within the centre of the fibre. If the failure stress of the fibre is σ_{failure} , then the stress is unable to reach the value needed to fracture the fibre. As a result, straining of a composite with short fibres will generally cause failure away from the fibre itself, possibly within the matrix or at the fibre–matrix boundary. A longer fibre may be of sufficient length to just cause failure in the fibre, with this length often referred to as the critical fibre length or l_c .

The critical fibre length can also be used as an indication of the level of adhesion between the fibre and the surrounding polymer matrix in a composite material. A weak interfacial strength will cause the stress profile to build up slowly along the fibre length, resulting in large l_c values, whereas very strong fibre–matrix interfaces cause a rapid rise in the tensile stress in the fibre during composite straining, resulting in relatively small l_c values. This relationship between the critical fibre length, the interfacial strength τ_c and the fracture stress of the fibre σ_f has been determined empirically (Kelly & Tyson 1965) as

$$l_c = \frac{\sigma_f d}{2\tau_c}. \quad (1.1)$$

The relationship between the fibre diameter and the critical length (l_c) importantly indicates how smaller diameters can improve the efficiency of polymer reinforcement. In this paper, we discuss one of the most common types of nanofibrous materials, carbon nanotubes (CNTs), and their importance in polymer composites.

2. Carbon nanotubes and their composites

CNTs (Iijima 1991) are a hexagonal network of carbon atoms rolled up to make a seamless cylinder. CNTs exist in two forms: single-wall nanotubes that possess the fundamental cylindrical structure and multi-wall nanotubes (MWNTs) that are

made up of two or more coaxial cylinders, with spacing between the layers close to that of the interlayer distance in graphite (0.34 nm). This structure is particularly unique and results in outstanding mechanical properties. Several groups have prepared macroscopic yarns or ropes consisting entirely of CNTs by direct spinning of such aligned arrays (Zhu *et al.* 2002; Ericson *et al.* 2004; Zhang *et al.* 2004a; Motta *et al.* 2005). However, while the nanotube alignment is good, the maximum reported tensile strength of such yarns was only 1.46 GPa (Motta *et al.* 2005), which is significantly lower than the maximum values of approximately 100 GPa (Yu *et al.* 2000; Barber *et al.* 2005) obtained from direct individual carbon nanotube testing. These results indicate that significant inter-tube sliding occurs within the carbon nanotube ropes during application of a force and emphasizes the need for a polymer matrix to bind the nanotubes together.

The reinforcing ability of CNTs in a polymer matrix can be quantitatively described using simple analytical models of which the Cox–Krenchel (Hull & Clyne 1981) is widely used. This simple treatment of the elastic behaviour of aligned long fibre composites is based on the premise that the ‘equal strain’ condition is valid for loading along the fibre axis. The axial Young’s modulus of the composite, E_c , can be written using the well-known rule of mixtures

$$E_c = V_f E_f + (1 - V_f) E_m, \quad (2.1)$$

where E_m and E_f are Young’s modulus of the matrix and the fibre, respectively, and V_f is the volume fraction of the fibre. Equation (2.1) highlights the importance of using high-stiffness reinforcing fibres aligned along the loading direction within the composite materials. The CNTs have been shown to have Young’s modulus of the order of 1 TPa (Treacy *et al.* 1996; Wong *et al.* 1997; Lourie & Wagner 1998; Salvetat *et al.* 1999a,b; Barber *et al.* 2005, 2006); thus only small volume fractions are needed to reinforce polymers that typically have Young’s modulus of 1–10 GPa.

For composites in which discontinuous fibres are not perfectly aligned, two parameters need to be incorporated in the equation, the length efficiency factor, η_L , and the orientation factor, η_0 :

$$E_c = \eta_L \eta_0 V_f E_f + (1 - V_f) E_m. \quad (2.2)$$

The fibre length efficiency factor η_L can vary between 0 and 1. The orientation factor η_0 is equal to 1 for fully aligned fibres, 3/8 for random two-dimensional orientation and 1/5 for three-dimensional orientation. A similar equation is valid for strength:

$$\sigma_c = \eta_L \eta_0 \sigma_f V_f + (1 - V_f) \sigma_m. \quad (2.3)$$

Equations (2.2) and (2.3) can be used to calculate the nanotube contribution to the composite properties if the mechanical properties of the matrix, the composite and the volume fractions are known.

Previous works have generally examined the mechanical performance of composites. Table 1 summarizes various carbon nanotube–polymer composites reported in the literature. The effective Young’s moduli of the CNTs are calculated using the respective volume fractions, composite Young’s modulus and equation (2.1). Large calculated carbon nanotube Young’s modulus values that approach the values of individual CNTs (approx. 1 TPa) indicate that the nanotubes are both highly aligned along the axis of the applied load and well

Table 1. List of the calculated Young's modulus and strength of the CNTs reinforcing various polymer matrices using equations (2.2) and (2.3).

type of CNTs	matrix	E_{NT} (GPa)	σ_{NT} (GPa)	reference
SWNTs	pitch	1269	13	Andrews <i>et al.</i> (1999)
MWNTs	UHMW-PE	868	4	Ruan <i>et al.</i> (2006)
SWNTs	PP	610	56	Kearns & Shambaugh (2002)
SWNTs	PBO	449	19	Kumar <i>et al.</i> (2002 <i>a,b</i>)
SWNTs	PVA	406	8	Zhang <i>et al.</i> (2004 <i>b</i>)
SWNTs	PA	153	36	Gao <i>et al.</i> (2005)
SWNTs	PAN	149	2	Sreekumar <i>et al.</i> (2004)
SWNTs	PAN	149	2	Chae <i>et al.</i> (2006)
SWNTs	PVA	147	3	Dalton <i>et al.</i> (2003)
MWNTs	PP	134	5	Kumar <i>et al.</i> (2002 <i>b</i>)
MWNTs	PAN	110	6	Chae <i>et al.</i> (2006)
DWNTs	PAN	61	2	Chae <i>et al.</i> (2006)
SWNTs	PMMA	55	—	Haggenmueller <i>et al.</i> (2000)
MWNTs	PC	48	−11	Pötschke <i>et al.</i> (2005)
MWNTs	PC	48	1	Fornes <i>et al.</i> (2006)
MWNTs	PP	29	—	Andrews <i>et al.</i> (2002)
SWNTs	PC	22	0	Fornes <i>et al.</i> (2006)
CNTs	PA	18	—	Sandler <i>et al.</i> (2004)
CNTs	PA	12	—	Sandler <i>et al.</i> (2004)
CNTs	PA	4	—	Sandler <i>et al.</i> (2004)
MWNTs	PVA	850	—	this work

dispersed, overcoming the sliding between the nanotubes, which lowers Young's modulus as in the case of carbon nanotube yarns and ropes (Zhu *et al.* 2002; Ericson *et al.* 2004; Zhang *et al.* 2004*a*; Motta *et al.* 2005). Recent literature reveals that solution cast films and especially solid drawing of polymer tapes (Ciselli 2007; Wang *et al.* 2007) give the highest carbon nanotube reinforcement in terms of Young's modulus and tensile strength using single-wall CNTs incorporated into polyvinyl alcohol (PVA). Conversely, some composites can be poorly manufactured such that the addition of CNTs as large aggregates can act as points of stress concentration resulting in a lowering of composite mechanical properties relative to the unreinforced polymer. This reduction in the mechanical properties is shown as a negative value in table 1.

The calculated values of Young's modulus and tensile strength of CNTs given in table 1 are predominantly lower than the experimentally measured values of isolated CNTs (Treacy *et al.* 1996; Wong *et al.* 1997; Lourie & Wagner 1998; Salvetat *et al.* 1999*a,b*; Barber *et al.* 2005, 2006). This highlights how the mechanical properties of the CNTs incorporated into polymer composites are rarely exploited. Reasons for the poor reinforcing ability in polymer composites are due to difficulty in achieving a homogeneous dispersion of nanotubes in the matrix, the quality of the nanotube–matrix interface and the potentially poor alignment of nanotubes along the loading direction. The relationship between calculated tensile strength and Young's modulus is complex and is strongly affected by variations in the nanotube alignment, dispersion and the type of

carbon nanotube used. While dispersion and the alignment of CNTs are often strongly affected by composite processing conditions, the nanotube-matrix interface is a more inherent composite property and requires more detail.

3. Nanotube adhesion

Direct testing of simple carbon nanotube-polymer composites has been used to quantify and isolate the interfacial adhesion between individual CNTs and polymer matrices. Cooper *et al.* (2002) fabricated thin epoxy films containing multi-wall and bundles of single-wall CNTs. The CNTs were found to bridge voids in the film so that most of the length of the nanotubes was bridging and a relatively small amount of the length embedded within the epoxy film. An atomic force microscope (AFM) was used to laterally deflect an individual nanotube until the embedded length was 'dragged out' of the polymer film. The largest recorded interfacial adhesion strengths in these experiments were an order of magnitude greater than the typical engineering composite values, indicating excellent polymer adhesion to the nanotubes, although the large variability in the interfacial strength (35–376 MPa) suggests the occurrence of potentially different failure events. Barber *et al.* (2003) attached individual CNTs to the end of an AFM tip and pushed the nanotube into a liquid copolymer, followed by solidification of the polymer, to produce single carbon nanotube composites. The nanotube was then pulled from the polymer matrix and the critical force required for interfacial failure was recorded by the AFM. Further experiments visualized this process by observing within a scanning electron microscope (SEM; Barber *et al.* 2006), as shown in figure 2.

All results showed a consistently high interfacial adhesion between the nanotube and the polymers used. In addition, fracture mechanics approaches have also shown that significant energy is required to debond the nanotube from a polymer (Barber *et al.* 2004*a,b*). The effect of inducing strong chemical bonding has also been investigated by modification of the carbon nanotube surfaces prior to individual carbon nanotube pull-out experiments (Barber *et al.* 2006). The authors used equation (1.1) to determine how the critical fibre length of approximately 1400 nm was significantly reduced to approximately 400 nm due to the chemical modification. It is important to note that the stresses developed in the polymer next to the nanotube during these tests are calculated to be far in excess of failure stresses of the bulk polymer material. Preferential crystallization of a higher modulus polymer interphase region at the nanotube surface during composite processing has been proposed as a possible explanation for the durability of this interface during composite loading (Ryan *et al.* 2007). However, individual carbon nanotube experiments have also measured high stresses at the interface using amorphous polymers.

4. Criteria for simple composite tests

The properties of a carbon nanotube composite have been shown to be critically dependent on the dispersion of the nanotubes within a polymer matrix, the alignment along the principal axis of applied force and the interfacial adhesion between the reinforcement and the polymer matrix. In order to examine these

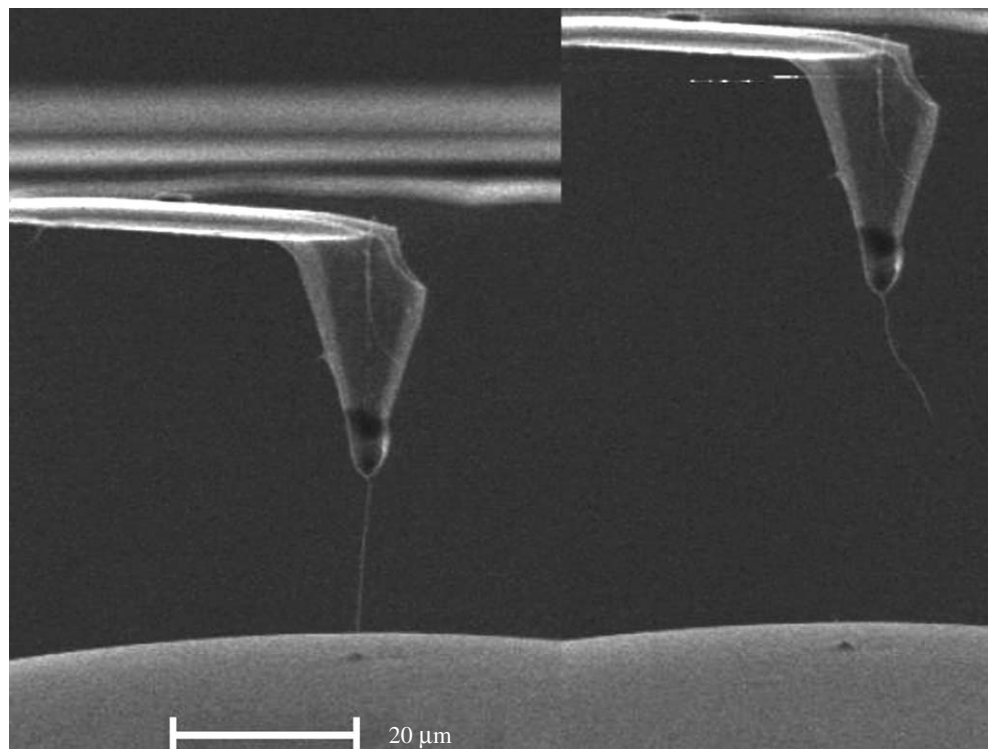


Figure 2. An individual carbon nanotube is attached to the end of an AFM probe and embedded within a solid epoxy polymer. Separation of the probe from the polymer causes pull-out of the nanotube (right) with the force recorded from the bending of the AFM cantilever.

parameters further, a simple carbon nanotube model composite is manufactured and mechanical testing performed to assess the validity of equation (2.1) and evaluate the true reinforcing ability of the CNTs in polymers. The production of polymer fibres reinforced with the CNTs is an effective system to study as the uncertainty in alignment can be overcome. Electrospinning of polymer nanofibres is a particularly effective manufacturing process (Dror *et al.* 2003; Zhou *et al.* 2005) for a model composite as the nanotubes themselves are constrained within the polymer volume and, if the length of the polymer fibre is very long but the diameter is small, will preferentially align along the principal fibre axis. Dispersion of the CNTs is problematic and is often overcome by the chemical modification of the nanotube surface. In this study, we use a commercially available surfactant, sodium dodecyl sulphate (SDS), to disperse the nanotubes in the polymer solution prior to the electrospinning process.

5. Sample preparation

A solution of PVA was prepared by dissolving granules of PVA ($M_w = 85\,000$ – $146\,000$; Aldrich, UK) in distilled water at 80°C for 2 hours. An amount of 0.021 g of multi-wall CNTs (Nanocyl, Bel.) was dispersed in 10 g of distilled water with 0.2 g of SDS (Aldrich, UK) and sonicated for 40 min until a

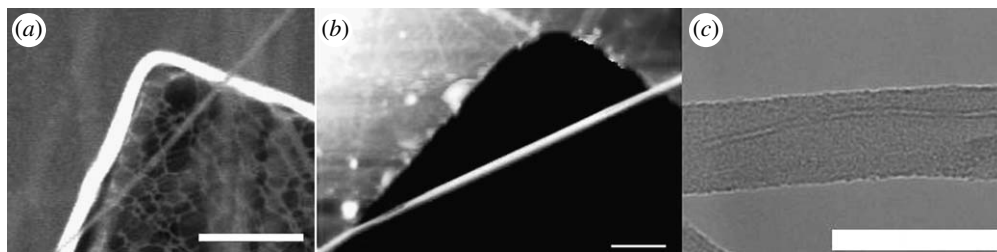


Figure 3. (a) SEM image of electrospun PVA nanofibres collected on a copper TEM grid (scale bar, 10 μm). (b) The corresponding AFM image (scale bar, 2 μm). (c) TEM image of an individual electrospun PVA-multi-wall carbon nanotube nanofibre (scale bar, 100 nm).

homogenous solution was observed. The MWNT solution was then added to 40 g of the PVA solution. In addition, solutions containing only PVA and SDS were prepared as a control. Electrospinning was performed using a 10 ml plastic syringe and a 17 gauge (inner diameter = 0.686 mm) stainless steel needle that was connected to a high-voltage supply (Glassman, UK), as described earlier (Doshi & Reneker 1995). The polymer solutions were flowed into the syringe using a syringe pump (Harvard Apparatus-PHD 2000, USA). Polymer fibres were electrospun onto an electrically grounded substrate 10 cm below the stainless steel needle by applying a voltage of 10–13 kV. A standard transmission electron microscope (TEM) copper grid (Agar Scientific, UK) was used as the substrate.

6. Results

The collected electrospun polymer fibres were imaged using an SEM (FEG-SEM JSM-6300F, JEOL, UK), an AFM in semi-contact mode (NTegra, NT-MDT, Rus.) and a TEM (JEM 2010, JEOL, UK). Figure 3 shows images of the corner of the TEM copper grid where a single polymer nanofibre has been deposited during the electrospinning process.

The images indicate that the electrospun polymer fibre has a consistent fibre diameter and is relatively taut while bridging the gap. Higher magnification TEM images of the polymer nanofibres bridging the grid holes are shown in figure 3. Despite the poor contrast between the CNTs and the surrounding PVA matrix material, the best contrast is seen between the hollow interior of the nanotube and the PVA; figure 3 shows the presence of aligned nanotubes within the polymer itself. This composite is therefore a simple model system where the CNTs can be seen to be well dispersed with a good alignment along the principal polymer nanofibre axis.

7. Nanomechanical testing

The image in figure 3 was used to position the AFM probe for subsequent nanomechanical bending of the polymer nanofibres and Young's modulus determination. This test is analogous to the three-point bending test. Owing to the imaging and nanomechanical testing being performed with the same AFM

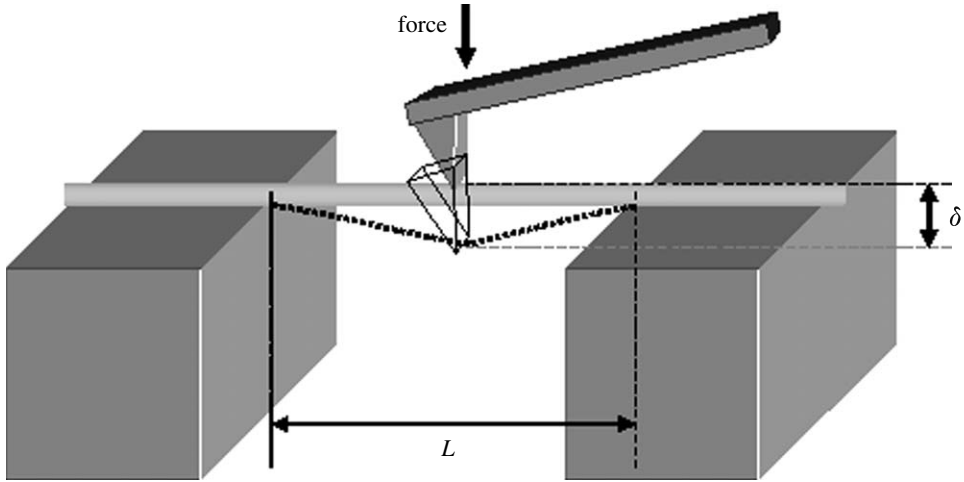


Figure 4. Schematic of the nanomechanical three-point bending test applied to bridging electrospun polymer nanofibres.

probe, an optimal AFM cantilever spring constant of approximately 1 N m^{-1} is found to be most effective. For nanomechanical testing, the AFM probe is positioned above the middle of the free length of the bridging nanofibre length and a contact mode force–distance curve obtained. A schematic of the test is shown in figure 4.

Positioning and spatial stability of the AFM probe are critical in performing accurate nanomechanical tests. For this reason, the AFM used a closed-loop system for accurate AFM probe placement. A drift rate of less than 4 nm h^{-1} ensures that, following the imaging of the sample in figure 3, the midpoint of the bridging nanofibre can be selected with certainty. The resultant bending test force–distance plots for electrospun PVA nanofibres, PVA nanofibres with SDS and PVA nanofibres with SDS and MWNTs are shown in figure 5. Briefly, the AFM probe is brought into contact with the bridging nanofibre (defined as the zero point on the fibre deflection axis) followed by a defined extension of the AFM z -piezo to push the probe into the nanofibre and cause it to bend. This bending strains the whole nanofibre composite length and therefore deforms both the PVA matrix and the CNTs contained within the whole bridging length. AFM cantilevers were accurately calibrated in order to convert cantilever bending into applied force using the Sader method (Sader *et al.* 1999). The fibre deflection δ is obtained using $\delta = (Z - Z_0) - b_{\text{cantilever}}$, where Z is the absolute z -piezo extension; Z_0 is the initial z -piezo extension upon probe contact; and $b_{\text{cantilever}}$ is the bending of the cantilever at Z .

8. Discussion

Figure 5 clearly shows that the addition of SDS reduces the stiffness of the electrospun polymer nanofibre with the CNTs added to the polymer nanofibres giving a significant increase in the applied force required to deflect the nanofibre. The linear nature of the plots indicates elastic behaviour in all cases and shows

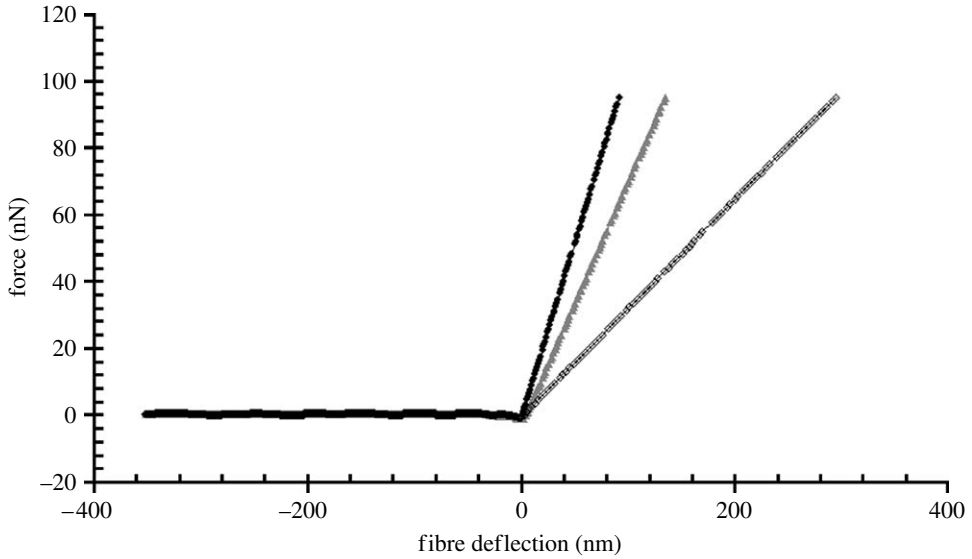


Figure 5. Typical plot of applied force against nanofibre deflection during nanomechanical testing using an AFM. Note that a negative fibre deflection indicates the AFM probe is away from the fibre and not applying any force. Filled triangles, PVA; open diamonds, PVA-SDS; filled diamonds, PVA-SDS-MWNT.

that slippage between the polymer nanofibres and the copper grid substrate, which would cause deviation from this linear response, does not occur for the relatively small deflections examined. Young's modulus E_f of each testing nanofibre could be calculated using (Timoshenko & Gere 1972)

$$E_f = \frac{F}{\delta} \frac{L^3}{192I}, \quad (8.1)$$

where F is the applied force to cause deflection of the nanofibre δ of bridging length L and I is the moment of inertia, defined for a cylindrical beam of diameter D as $I = (\pi D^4)/64$. This equation is very effective for free length-to-diameter ratios greater than 16 as shown in figure 3. Bending of fibres below this ratio is more complicated as shear forces within the bending fibre can become significant. A linear relationship between the applied force and the nanofibre deflection upon contact of the AFM probe with the bridging nanofibre has been previously observed, indicating elastic behaviour, and modelled using the elastic beam bending theory of equation (8.1) (Tan & Lim 2004; Shin *et al.* 2006; Xiong *et al.* 2006). The use of elastic beam bending theory is accurate only at small fibre deflections where the angle made by the bending fibre in relation to the horizontal plane is less than 5° . Fibre deflections beyond this point give a transition from fibre bending to tensile elastic deformation of the fibre's free length and give a deviation from a linear fibre deflection versus applied force plot (Heidelberg *et al.* 2006). The linear relationship in figure 5 and inspection of the fibre deflection values (less than 200 nm) relative to the free suspended nanofibre lengths of approximately $10 \mu\text{m}$ correlate with the previous work, highlighting how the nanofibres are deflected by small amounts corresponding to the bending regime.

Table 2. Calculated Young's modulus of various electrospun polymer nanofibres using equation (8.1).

fibres system	average L/D ratio	E (GPa)
PVA	34.7	7.12 ± 1.07
PVA–SDS	37.6	6.46 ± 0.97
PVA–SDS–MWNT	31.5	9.87 ± 1.47

Three nanofibre bending tests were performed on each of the three nanofibre combinations and the results are shown in table 2, which show that while SDS does appear to change Young's modulus of PVA nanofibres, the PVA modulus with and without the SDS is still quite high, suggesting that the PVA molecules are highly aligned during the electrospinning process. Indeed, the low molecular weight of SDS would be expected to reduce Young's modulus of most polymers. The addition of MWNTs increases Young's modulus of the resultant fibres by approximately 50%. As the system studied is close to a model composite, equation (2.1) can be applied to examine the reinforcing contribution of the CNTs to PVA. This assumption is not perfect as the carbon nanotube lengths are not continuous along the polymer nanofibre length. We would therefore expect values from this short fibre reinforcing effect to be a lower boundary. The volume fraction for the CNTs can be estimated to be approximately 0.4% from sample preparation. Using an E_m value of the PVA–SDS gives a calculated effective Young's modulus of the carbon nanotube as 0.85 TPa or an expected composite Young's modulus of 10.5 GPa. The experimentally measured Young's modulus of the carbon nanotube–PVA composite is very close to the theoretical E_c based on a PVA–SDS modulus of 6.46 GPa and a carbon nanotube modulus of 1 TPa. This highlights the effectiveness of the CNTs as reinforcements in polymers due to two main reasons. First is the lack of bundling of nanotubes owing to the SDS dispersant. Second, the alignment of CNTs along the polymer fibre principal axis is achieved (figure 3) as the carbon nanotube length is much longer than the polymer nanofibre diameter, forcing the nanotube to be governed by the restricted geometry of the polymer. The validity of equation (2.1) in our work is interesting as it suggests that there is an isostrain condition between the PVA matrix and the CNTs, indicating a strong interfacial adhesion.

Potential differences in the morphology of the PVA–SDS due to the inclusion of CNTs may cause some error in the selected value of E_m . In a previous study, Ryan *et al.* (2007) reported that Young's modulus of the PVA–MWNT cast film increased as the polymer crystallinity increased. MWNTs were seen to nucleate polymer crystal growth and this crystal structure was proposed as the dominant reinforcement. Similar results were also shown in other studies of semi-crystalline polymer–carbon nanotube bulk systems (Bhattacharyya *et al.* 2003; Coleman *et al.* 2004; Ciselli 2007). However, no direct visualization of preferential polymer morphology at a nanotube surface has been reported in the literature, unless using highly specific processing conditions using an individual nanotube (Barber *et al.* 2004*a,b*). Since the electrospun polymer fibres in our study are different from the bulk film systems prepared in the literature, the potential differences of polymer structure in the electrospun nanofibres must be highlighted.

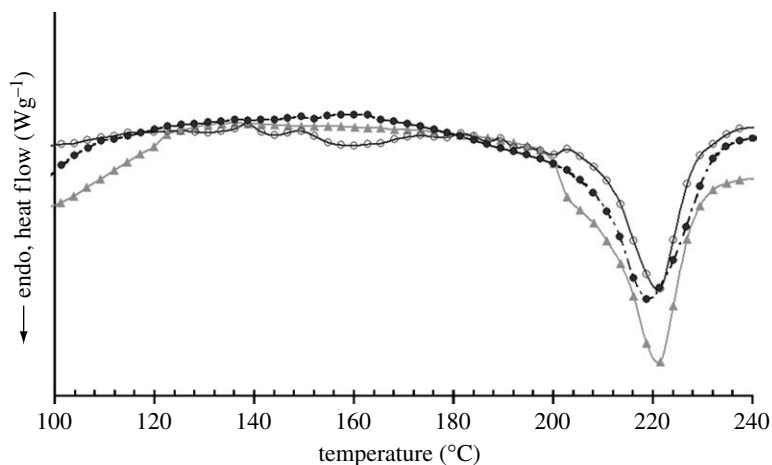


Figure 6. DSC melting thermograms during the first heating scans for three electrospun fibres, showing no significant difference in polymer in PVA-SDS to PVA-SDS-MWNT. Filled triangles, PVA; open circles, PVA-SDS; filled circles, PVA-SDS-MWNT.

To support this hypothesis, we measured the melting peaks during first heating scans for three different electrospun fibre combinations (PVA, PVA + SDS and PVA + SDS + MWNT) using differential scanning calorimetry (DSC¹). The DSC thermograms are shown in figure 6. The results show little difference in the shape or position of the polymer melt peak from PVA-SDS to PVA-SDS-MWNT, with the latter peak position approximately 1°C lower than the former. The sharp peak of the pure PVA visually indicates it is the most crystalline structure, which is contrary to the results as shown by Ryan *et al.* (2007) and highlights the difference between electrospun polymers and cast films. Thus, in the electrospun PVA-SDS-MWNT fibres, the mechanical reinforcement is predominantly due to the good dispersion, orientation of nanotubes within the polymer and the potentially strong interfacial adhesion (Barber *et al.* 2003; Zhou *et al.* 2005; Liu *et al.* 2007), and not notably dependent on PVA morphology.

9. Conclusions

CNTs have excellent mechanical properties and significant potential for reinforcing polymer composites. Numerous studies have examined the mechanical performance of carbon nanotube-polymer composites with a large variability in the effectiveness of the carbon nanotube reinforcing ability. A rule of mixtures approach can be used to assess the reinforcement behaviour, with an effective Young's modulus of the carbon nanotube being characteristic of the alignment and the dispersion of the nanotube in the polymer. Simple carbon nanotube-polymer composites are produced using an electrospinning process to examine the potential nanotube reinforcements. Three-point bending tests using an AFM are valuable

¹DSC measurements of three electrospun fibre mats were performed on a METTLER TOLEDO DSC (model 822^e) in an air nitrogen atmosphere. The samples were heated from 0 to 250°C at a heating rate of 40°C min⁻¹ to avoid the potential thermal degradation of the polymer samples. As the fibres would be melted to liquid over T_m , we only measured the first heating scans for all three samples.

in determining the mechanical properties of individual electrospun nanofibres containing CNTs. Importantly, SDS employed to increase the dispersion of the CNTs was shown to lower Young's modulus of the resultant carbon nanotube–PVA composite fibres. By taking the effect of the SDS on PVA matrix mechanical properties into account, the improvement of composite properties due to the addition of CNTs can be examined, although further potential modification of the PVA–SDS structure due to the addition of CNTs is required. Calculations show that the addition of CNTs is in good agreement with the expected Young's modulus for dispersed, highly aligned fibre reinforced composites indicating effective bonding between the reinforcement and the polymer matrix.

References

- Andrews, R., Jacques, D., Rao, A. M., Rantell, T., Derbyshire, F., Chen, Y., Chen, J. & Haddon, R. C. 1999 Nanotube composite carbon fibers. *Appl. Phys. Lett.* **75**, 1329–1331. (doi:10.1063/1.124683)
- Andrews, R., Jacques, D., Minot, M. & Rantell, T. 2002 Fabrication of carbon multiwall nanotube/polymer composites by shear mixing. *Macromol. Mater. Eng.* **287**, 395–403. (doi:10.1002/1439-2054(20020601)287:6<395::AID-MAME395>3.0.CO;2-S)
- Barber, A. H., Cohen, S. R. & Wagner, H. D. 2003 Measurement of carbon nanotube–polymer interfacial strength. *Appl. Phys. Lett.* **82**, 4140–4142. (doi:10.1063/1.1579568)
- Barber, A. H., Cohen, S. R. & Wagner, H. D. 2004a Stepped polymer morphology induced by a carbon nanotube tip. *Nano Lett.* **4**, 1439–1443. (doi:10.1021/nl049281p)
- Barber, A. H., Cohen, S. R., Kenig, S. & Wagner, H. D. 2004b Interfacial fracture energy measurements for multi-walled carbon nanotubes pulled from a polymer matrix. *Compos. Sci. Technol.* **64**, 2283–2289. (doi:10.1016/j.compscitech.2004.01.023)
- Barber, A. H., Andrews, R., Schadler, L. S. & Wagner, H. D. 2005 On the tensile strength distribution of multiwalled carbon nanotubes. *Appl. Phys. Lett.* **87**, 203 106. (doi:10.1063/1.2130713)
- Barber, A. H., Cohen, S. R., Eitan, A., Schadler, L. S. & Wagner, H. D. 2006 Fracture transitions at a carbon-nanotube/polymer interface. *Adv. Mater.* **18**, 83–87. (doi:10.1002/adma.200501033)
- Bhattacharyya, A. R., Sreekumar, T. V., Liu, T., Kumar, S., Ericson, L. M., Hauge, R. H. & Smalley, R. E. 2003 Crystallization and orientation studies in polypropylene/single wall carbon nanotube composite. *Polymer* **44**, 2373–2377. (doi:10.1016/S0032-3861(03)00073-9)
- Chae, H. G., Minus, M. L. & Kumar, S. 2006 Oriented and exfoliated single wall carbon nanotubes in polyacrylonitrile. *Polymer* **47**, 3494–3504. (doi:10.1016/j.polymer.2006.03.050)
- Ciselli, P. 2007 The potential of carbon nanotubes in polymer composites. PhD thesis, Eindhoven University of Technology.
- Coleman, J. N. et al. 2004 High performance nanotube-reinforced plastics: understanding the mechanism of strength increase. *Adv. Funct. Mater.* **14**, 791–798. (doi:10.1002/adfm.200305200)
- Cooper, C. A., Cohen, S. R., Barber, A. H. & Wagner, H. D. 2002 Detachment of nanotubes from a polymer matrix. *Appl. Phys. Lett.* **81**, 3873–3875. (doi:10.1063/1.1521585)
- Dalton, A. B., Collins, S., Muñoz, E., Razal, J. M., Ebron, V. H., Ferraris, J. P., Coleman, J. N., Kim, B. G. & Baughman, R. H. 2003 Supertough carbon-nanotube fibres. *Nature* **423**, 703. (doi:10.1038/423703a)
- Doshi, J. & Reneker, D. H. 1995 Electrospinning process and applications of electrospun fibers. *J. Electrostat.* **35**, 151–160. (doi:10.1016/0304-3886(95)00041-8)
- Dror, Y., Salalha, W., Khalfin, R. L., Cohen, Y., Yarin, A. L. & Zussman, E. 2003 Carbon nanotubes embedded in oriented polymer nanofibers by electrospinning. *Langmuir* **19**, 7012–7020. (doi:10.1021/la034234i)
- Ericson, L. M. et al. 2004 Macroscopic, neat, single-walled carbon nanotube fibers. *Science* **305**, 1447–1450. (doi:10.1126/science.1101398)

- Fornes, T. D., Baur, J. W., Sabba, Y. & Thomas, E. L. 2006 Morphology and properties of melt-spun polycarbonate fibers containing single- and multi-wall carbon nanotubes. *Polymer* **47**, 1704–1714. (doi:10.1016/j.polymer.2006.01.003)
- Gao, J., Itkis, M. E., Yu, A., Bekyarova, E., Zhao, B. & Haddon, R. C. 2005 Continuous spinning of a single-walled carbon nanotube-nylon composite fiber. *J. Am. Chem. Soc.* **127**, 3847–3854. (doi:10.1021/ja0446193)
- Haggenmueller, R., Gommans, H. H., Rinzler, A. G., Fischer, J. E. & Winey, K. I. 2000 Aligned single-wall carbon nanotubes in composites by melt processing methods. *Chem. Phys. Lett.* **330**, 219–225. (doi:10.1016/S0009-2614(00)01013-7)
- Heidelberg, A., Ngo, L. T., Wu, B., Phillips, M. A., Sharma, S., Kamins, T. I., Sader, J. E. & Boland, J. J. 2006 A generalized description of the elastic properties of nanowires. *Nano Lett.* **6**, 1101–1106. (doi:10.1021/nl060028u)
- Hull, D. & Clyne, T. 1981 *An introduction to composite materials*. Cambridge, UK: Cambridge University Press.
- Iijima, S. 1991 Helical microtubules of graphitic carbon. *Nature* **354**, 56. (doi:10.1038/354056a0)
- Kearns, J. C. & Shambaugh, R. L. 2002 Polypropylene fibers reinforced with carbon nanotubes. *J. Appl. Polym. Sci.* **86**, 2079–2084. (doi:10.1002/app.11160)
- Kelly, A. & Tyson, W. R. 1965 Tensile properties of fibre-reinforced metals. copper/tungsten and copper/molybdenum. *Mech. Phys. Solids* **13**, 329–338. (doi:10.1016/0022-5096(65)90035-9)
- Kumar, S. *et al.* 2002a Synthesis, structure, and properties of PBO/SWNT composites. *Macromolecules* **35**, 9039–9043. (doi:10.1021/ma0205055)
- Kumar, S., Doshi, H., Srinivasarao, M., Park, J. O. & Schiraldi, D. A. 2002b Fibers from polypropylene/nano carbon fiber composites. *Polymer* **43**, 1701–1703. (doi:10.1016/S0032-3861(01)00744-3)
- Liu, L.-Q., Tasis, D., Prato, M. & Wagner, H. D. 2007 Tensile mechanics of electrospun multiwalled nanotube/poly(methyl methacrylate) nanofibers. *Adv. Mater.* **19**, 1228–1233. (doi:10.1002/adma.200602226)
- Lourie, O. & Wagner, H. D. 1998 Evaluation of Young's modulus of carbon nanotubes by micro-Raman spectroscopy. *J. Mater. Res.* **13**, 2418–2422. (doi:10.1557/JMR.1998.0336)
- Motta, M., Li, Y.-L., Kinloch, I. & Windle, A. 2005 Mechanical properties of continuously spun fibers of carbon nanotubes. *Nano Lett.* **5**, 1529–1533. (doi:10.1021/nl050634+)
- Pötschke, P., Brünig, H., Janke, A., Fischer, D. & Jehnichen, D. 2005 Orientation of multiwalled carbon nanotubes in composites with polycarbonate by melt spinning. *Polymer* **46**, 10 355–10 363. (doi:10.1016/j.polymer.2005.07.106)
- Ruan, S., Gao, P. & Yu, T. X. 2006 Ultra-strong gel-spun UHMWPE fibers reinforced using multiwalled carbon nanotubes. *Polymer* **47**, 1604–1611. (doi:10.1016/j.polymer.2006.01.020)
- Ryan, K. P. *et al.* 2007 Carbon nanotubes for reinforcement of plastics? a case study with poly(vinyl alcohol). *Compos. Sci. Technol.* **67**, 1640–1649. (doi:10.1016/j.compscitech.2006.07.006)
- Sader, J. E., Chon, J. W. M. & Mulvaney, P. 1999 Calibration of rectangular atomic force microscope cantilevers. *Rev. Sci. Instrum.* **70**, 3967–3969. (doi:10.1063/1.1150021)
- Salvetat, J.-P., Briggs, G. A. D., Bonard, J.-M., Bacsá, R. R., Kulik, A. J., Stöckli, T., Bunham, N. A. & Forró, L. 1999a Elastic and shear moduli of single-walled carbon nanotube ropes. *J. Phys. Rev. Lett.* **82**, 944–947. (doi:10.1103/PhysRevLett.82.944)
- Salvetat, J.-P. *et al.* 1999b Elastic modulus of ordered and disordered multiwalled carbon nanotubes. *Adv. Mater.* **11**, 161–165. (doi:10.1002/(SICI)1521-4095(199902)11:2<161::AID-ADMA161>3.0.CO;2-J)
- Sandler, J. K. W. *et al.* 2004 A comparative study of melt spun polyamide-12 fibres reinforced with carbon nanotubes and nanofibres. *Polymer* **45**, 2001–2015. (doi:10.1016/j.polymer.2004.01.023)
- Shin, M. K., Kim, S. I., Kim, S. J., Kim, S.-K. & Lee, H. 2006 Reinforcement of polymeric nanofibers by ferritin nanoparticles. *Appl. Phys. Lett.* **88**, 193 901. (doi:10.1063/1.2200469)

- Sreekumar, T. V., Liu, T., Min, B. G., Guo, H., Kumar, S., Hauge, R. H. & Smalley, R. E. 2004 Polyacrylonitrile single-walled carbon nanotube composite fibers. *Adv. Mater.* **16**, 58–61. (doi:10.1002/adma.200305456)
- Tan, E. P. S. & Lim, C. T. 2004 Physical properties of a single polymeric nanofiber. *Appl. Phys. Lett.* **84**, 1603–1605. (doi:10.1063/1.1651643)
- Timoshenko, S. P. & Gere, J. M. 1972 *Mechanics of materials*. New York, NY: Van Nostrand.
- Treacy, M. M., Ebbesen, T. W. & Gibson, L. M. 1996 Exceptionally high Young's modulus observed for individual carbon nanotubes. *Nature* **381**, 678. (doi:10.1038/381678a0)
- Wang, Z., Ciselli, P. & Peijs, T. 2007 The extraordinary reinforcing efficiency of single-walled carbon nanotubes in oriented poly(vinyl alcohol) tapes. *Nanotechnology* **18**, 455709. (doi:10.1088/0957-4484/18/45/455709)
- Wong, E. W., Sheehan, P. E. & Lieber, C. M. 1997 Nanobeam mechanics: elasticity, strength, and toughness of nanorods and nanotubes. *Science* **277**, 1971–1975. (doi:10.1126/science.277.5334.1971)
- Xiong, Q., Duarte, N., Tadigadapa, S. & Eklund, P. C. 2006 Force-deflection spectroscopy: a new method to determine the Young's modulus of nanofilaments. *Nano Lett.* **6**, 1904–1909. (doi:10.1021/nl060978f)
- Yu, M.-F., Lourie, O., Dyer, M. J., Moloni, K., Kelly, T. F. & Ruoff, R. S. 2000 Strength and breaking mechanism of multiwalled carbon nanotubes under tensile load. *Science* **287**, 637–640. (doi:10.1126/science.287.5453.637)
- Zhang, M., Atkinson, K. R. & Baughman, R. H. 2004a Multifunctional carbon nanotube yarns by downsizing an ancient technology. *Science* **306**, 1358–1361. (doi:10.1126/science.1104276)
- Zhang, X., Liu, T., Sreekumar, T. V., Kumar, S., Hu, X. & Smith, K. 2004b Gel spinning of PVA/SWNT composite fiber. *Polymer* **45**, 8801–8807. (doi:10.1016/j.polymer.2004.10.048)
- Zhou, W., Wu, Y., Wei, F., Luo, G. & Qian, W. 2005 Elastic deformation of multiwalled carbon nanotubes in electrospun MWCNTs-PEO and MWCNTs-PVA nanofibers. *Polymer* **46**, 12 689–12 695. (doi:10.1016/j.polymer.2005.10.114)
- Zhu, H. W., Xu, C. L., Wu, D. H., Wei, B. Q., Vajtai, R. & Ajayan, P. M. 2002 Direct synthesis of long single-walled carbon nanotube strands. *Science* **296**, 884–886. (doi:10.1126/science.1066996)